CrystEngComm

Accepted Manuscript

This article can be cited before page numbers have been issued, to do this please use: K. A. Kokh, V. V. Atuchin, S. V. Adichtchev, T.A. Gavrilova, A.M. Bahadur , A.S. Klimov, I. V. Korolkov, N. Kuratieva, S. Mukherjee, N. V. Pervukhina and N. V. Surovtsev, *CrystEngComm*, 2020, DOI: 10.1039/D0CE01264E.

ROYAL SOCIETY OF CHEMISTRY

rsc.li/crystengcomm

Corresponding author: V.V. Atuchin
Institute of Semiconductor Physics, Novosibirsk 630090, Russia
Phone: +7 (383) 3308889
E-mail: atuchin@isp.nsc.ru

View Article Online
DOI: 10.1039/D0CE01264E

Cu_2ZnSnS_4 crystal growth using a $SnCl_2$ based flux

K.A. Kokh[1,2,*], V.V. Atuchin[3,4,5], S.V. Adichtchev[6], T.A. Gavrilova[7], A.M. Bakhadur[8], A.S. Klimov[1,2], I.V. Korolkov[9,10], N.V. Kuratieva[9,10], S. Mukherjee[11], N.V. Pervukhina[4,10], N.V. Surovtsev[6]

[1] Laboratory of Crystal Growth, Sobolev Institute of Geology and Mineralogy, SB RAS, Novosibirsk 630090, Russia

[2]Department of Geology and Geophysics, Novosibirsk State University, Novosibirsk 630090, Russia

[3]Laboratory of Optical Materials and Structures, Rzhanov Institute of Semiconductor Physics, SB RAS, Novosibirsk 630090, Russia

[4]Laboratory of Semiconductor and Dielectric Materials, Novosibirsk State University, Novosibirsk 630090, Russia

[5]Research and Development Department, Kemerovo State University, Kemerovo 650000, Russia

[6]Laboratory of Condensed Matter Spectroscopy, Institute of Automation and Electrometry, SB RAS, Novosibirsk 630090, Russia

[7]Laboratory of Nanodiagnostics and Nanolithography, Institute of Semiconductor Physics, SB RAS, Novosibirsk 630090, Russia

[8]Department of Chemistry and Chemical Technology, Al Farabi Kazakh National University, Alma Ata 050040, Kazakhstan

[9]Laboratory for Research Methods in Composition and Structure of Functional Materials, Novosibirsk State University, Novosibirsk 630090, Russia

[10]Laboratory of Crystal Chemistry, Nikolaev Institute of Inorganic Chemistry, SB RAS, Novosibirsk 630090, Russia

[11]Hybrid Nanodevice Research Group (HNRG), Electrical Engineering and Centre for Advanced Electronics (CAE), Indian Institute of Technology Indore, Madhya Pradesh 453552, India

View Article Online
DOI: 10.1039/D0CE01264E

Abstract

The stoichiometry and phase homogeneity of the kesterite type compound Cu_2ZnSnS_4 play a key role in its efficiency in solar cells. In this work, $CuCl_2$, $ZnCl_2$ and $SnCl_2$ were applied as solvents in the Cu_2ZnSnS_4 crystal growth for the first time. The multiphase ingot was obtained by a direct fusion of the stoichiometric batch composed of constituent elements. Compared to that, the material recrystallized in $SnCl_2$ presented the single phase Zn-rich kesterite with composition $Cu_{1.94}Zn_{1.06}SnS_4$ and unit cell parameters a = 5.4324(3) and c = 10.8383(2) Å. The crystal structure of $Cu_{1.94}Zn_{1.06}SnS_4$ was determined by a single crystal X-ray diffraction analysis. The integral phase purity of the crystals grown with the use of $SnCl_2$ solvent was verified by a powder X-ray diffraction analysis and Raman measurements. In the Raman spectrum, the FWHM value of the 337 cm^{-1} line was as low as 9.6 cm^{-1}, and that indicates the minimal lattice disorder.

Keywords: kesterite; crystal growth; flux; crystal structure; Raman

View Article Online
DOI: 10.1039/D0CE01264E

1. Introduction

At the present time, $Cu_2ZnSn(S,Se)_4$ (CZTSSe) compounds of the kesterite type structure are extensively investigated as promising absorbers in thin-film photovoltaic devices due to their large absorption coefficient (104 cm^{-1}), appropriate bandgap (1.0-1.5 eV) and earth abundant constituent elements [1-5]. It can be noted that, recently, similar absorber properties were also reported for the compounds with a general formula $Cu_2HgSn(Ge)S(Se)_4$ [6-9]. To date, the CZTSSe thin-film solar cells with a 10-12.6% conversion efficiency have been realized, and a further improvement of the CZTSSe-based solar cells can be assumed to reach their high theoretical efficiency of ~30% for single junction structures [10-14]. This further progress, however, is possible on the base of detailed investigation of physical and chemical properties of $Cu_2ZnSn(S,Se)_4$ compounds.

In thin film technologies, when the temperature is comparatively low and the compound layer is formed under essentially non-equilibrium conditions, the crystallinity, real defect structure and composition homogeneity are strongly determined by the deposition conditions, including the heating/cooling rates, reagents, geometry of an experimental setup and so on [1,2,12,15-17]. Respectively, the optimal deposition conditions should be determined to reach the film characteristics appropriate for the device structure optimization. As a rule, the best way for such optimization is the comparison of physical and chemical properties of the complex compound in the film form with those obtained for the same compound in the bulk crystal state, where the optical and electrical parameters can be measured as a function of crystallographic orientation.

In the CZTSSe-based thin-film solar cell production, one should account for the influence of inter diffusion between different deposited layers [18,19]. However, considering the absorber layer material, the crucial effect is brought about by the components with differing volatility and following nonreproducible stoichiometry [20-24]. In the case of kesterite film analysis, the comparison with the bulk crystal properties is particularly significant and, respectively, the high-quality of CZTSSe crystals growth is extremely valuable. In recent years, many technologies were

View Article Online
DOI: 10.1039/D0CE01264E

tested for the preparation of kesterite crystals [25-32], and the crystal growth from molten halide fluxes seems to be among the most promising methods [33]. In this technique, the crystallization temperature is significantly below the decomposition point known for CZTSSe compounds (Cu_2ZnSnS_4, ~500°C) [34-36]. Thus, the preparation of relatively big crystals, commonly without foreign phase capture, becomes possible with the use of KI or CdI_2 solvents [33,37]. However, in this case, the incorporation of foreign cations into the kesterite structure is possible [34]. To avoid this factor, the present work is aimed at the use of constituent element chlorides, $CuCl_2$, $ZnCl_2$ and $SnCl_2$, for the Cu_2ZnSnS_4 crystal growth. The chloride-based solvents seem to be more suitable than iodide compounds from the technological point of view because of their lower hygroscopicity and simple chemical preparation. With this approach, only chlorine may be a potential foreign impurity in the resulting kesterite compound, which will obviously decrease the number of factors to control the solar cell device production.

2. Experimental

All synthesis and flux crystallization procedures were carried out in fuzed quartz ampoules, since it is necessary to protect the molten material against oxidation. The ampoules were washed up with HNO_3 acid and bidistilled water. The starting materials were elementary Cu, Sn, S (Wuhan Xinrong New Materials Co. Ltd, 4N), Zn (Fox Chemicals, 4N) and CuO (Ural Chemical Reagent Plant, 99.9%). Initially the polycrystalline CZTS was synthesized. The CZTS ingot was prepared by the slow heating to 1050°C of the Cu, Zn, Sn and S materials mixed at the stoichiometric ratio. For homogenization, the melt with the formal CZTS composition was treated at 1050°C for 20 h and then cooled with the switched off furnace. The resulting ingot was crushed and the product was taken for three experiments with different fluxes. The flux components were prepared just before the ampoule sealing in order to minimize the water vapor capture from the air. $SnCl_2$ was obtained by heating $SnCl_2 \cdot 2H_2O$ (Alphaservice, 99.99%) in a ceramic cup at 200°C during 3 h. Zinc chloride and copper chloride (II) were obtained by dissolving metallic Zn and CuO, correspondingly, in

View Article Online
DOI: 10.1039/D0CE01264E

high purity chloric acid (Sigma Tek, 38%) and the following evaporation at 200°C in the air, and at 100°C under vacuum. The obtained $SnCl_2$ and $ZnCl_2$ products were white and $CuCl_2$ was brown. The phase composition of the synthesized metal chlorides was controlled by the powder XRD analysis (not shown).

For recrystallization experiments, 5 g of CZTS batches were put in three separate silica ampoules with dimensions 1x30 cm. In each case, the amount of added solvent was calculated on the base of 1/1 molar proportion to the CZTS quantity. The ampoules were sealed at residual pressure 5×10^{-3} Torr and heated in a horizontal muffle furnace to 900°C. After this, the ampoules were slowly cooled to 500°C with the ramp 1 K/h and then cooled down naturally with the switched off furnace. After breaking the ampoule, to remove the solvent component, the product was rinsed by water and ethanol. The undissolved precipitate was examined by X-ray diffraction, microscopic, EDS SEM and Raman analyses. In what follows, the samples obtained with the use of $CuCl_2$, $ZnCl_2$ and $SnCl_2$ are designated as **I**, **II** and **III**.

The chemical analyses were performed on a Tescan MIRA 3 LMU scanning electron microscope coupled with an INCA EDS 450 microanalyser. The SEM pattern of the sample applied in the Raman experiment was recorded with the use of a Hitachi SU8220 device.

The phase composition of grown crystals was obtained by the powder XRD analysis. The XRD patterns were recorded with the use of a Shimadzu XRD-7000 diffractometer (CuK-alpha radiation, Ni – filter, 2θ = 5-70°, 0.03° 2θ step, 1s per step). A polycrystalline sample was slightly ground with hexane in an agate mortar, and the resulting suspension was deposited on the polished side of a standard quartz sample holder to form a smooth thin layer after drying. The precision scans were performed for the sample obtained in $ZnCl_2$ and $SnCl_2$ fluxes: diffraction angle range 2θ = 10-120°, step 0.03° 2θ, 10s per step. Indexing the diffraction patterns was carried out using the data for the compounds reported in the PDF database [38]. The unit cell parameters were refined by using the Topas Academic v.6 software [39]. The peak profiles were described by the pseudo-Voigt function in the diffraction angle range of 2θ = 90–120°.

The single-crystal X-ray diffraction data for the selected sample grown with the use of $SnCl_2$ were collected on a Bruker Apex DUO CCD diffractometer equipped with the graphite monochromated MoKα (λ = 0.71073 Å) radiation at 293(2) K. The ω-scan technique was employed to measure intensities. The absorption corrections were applied empirically using the SADABS program [40]. The structure was solved by the direct methods of the difference Fourier synthesis and further refined by the full-matrix least squares method using the SHELXTL package [41]. The atomic thermal parameters for all atoms were refined anisotropically. The structure refinement shows the cooperative occupation of Cu and Zn atom positions. The self-occupancy factor (SOF) for Cu and Zn atoms in position Cu(2) was refined from the difference electron density maps and fixed at the ratio of 1.94/0.06 according to the chemical composition analysis.

The Raman experiment was performed at room temperature in the backscattering geometry by using a solid-state laser Millenia (Spectra Physics) with wavelength 532.1 nm and Raman spectrometer Trivista 777. The spectral resolution of the spectrometer was ~1 cm^{-1}. A neon-discharge lamp was used for the spectrometer wavelength calibration. A spherical lens with focal length 40 mm was used for focusing the laser beam onto the sample and collecting scattered light as well. The incident laser beam intensity at the sample was about 60 mW.

3. Results and discussions

To see the result of the CZTS synthesis, the obtained ingot was cut length wise and its inner surface was polished. Then, the polished surface was observed with an optical microscope Olympus BX53P with the illumination by white reflected light. The CZTS ingot obtained after the synthesis at 1050°C was visually inhomogeneous, as shown in Figure 1a. The presence of four phases was detected as a result of microscopic examination of the polished section and the phases were identified according to their chemical compositions determined by EDS measurements. The dominant part of the sample surface was occupied by the Cu_2ZnSnS_4 phase, and the remaining part - by ZnS, Cu_2SnS_3 and SnS. The lack of the contact between the ZnS and SnS grains is worth

View Article Online
DOI: 10.1039/D0CE01264E

noting. The structure of the quasi-binary ZnS-Cu_2SnS_3 diagram is known [42] and the relics of the ZnS and Cu_2SnS_3 phases can be explained by the incomplete peritectic reaction ZnS + L = Cu_2ZnSnS_4. However, a noticeable amount of the SnS phase in some parts of the ingot indicates a large deviation from equilibrium in the system, probably due to the component redistribution through the gas phase. Such an uneven distribution of the components in the ingot makes it difficult to obtain a single phase product, even with a very long subsequent solid phase annealing. It is known that the presence of a foreign phase significantly affects the performance of CZTS batteries [22]. As for the chemical composition of the CZTS phase, the measured cation ratios Cu/(Zn + Sn) ~ 1.03 and Zn/Sn ~ 1.05 (Table 1) lie outside the field of the desired CZTS compositions [23].

Therefore, the reduction of crystallization temperature and vapor pressure of the volatile components with the use of a flux seems to be a promising approach. In the growth experiments, the CZTS ingot pieces were sealed in separate ampoules with the constituent metal chloride salts. It could be mentioned that the melting points of the chlorides are significantly different: $CuCl_2$ (498°C), $ZnCl_2$ (318°C) and $SnCl_2$ (247°C) [43]. Respectively, the spontaneous crystallization on cooling is also assumed at different temperatures.

First, to reveal the most promising solvent type, the phase analysis of grown crystals **I**, **II** and **III** was implemented with the use of available literature information. In the case of $CuCl_2$ (Figure 1S), the Cu_2ZnSnS_4 phase formation was not detected. The presence of CuS (PDF 010-78-2121 [44]), ZnS (PDF 010-71-5976 [45]) (or CuCl (PDF 010-82-2114 [46]) and the phase isostructural to $Cu_{1.8}S$ (PDF 010-70-9132 [43]) were found in the washed sediment **I**. ZnS and CuCl crystals have the same symmetry (space group *F*-43*m*) and almost the same cell parameters. For this reason, the selection of the phase present in sample **I** is not possible by the methods of XRD analysis. Besides, it is not possible to identify the phase containing tin. Probably, it turned into a water-soluble form and then it was removed during the sample processing. Thus, the $CuCl_2$ solvent is not appropriate for the CZTS crystal growth.

DOI: 10.1039/D0CE01264E

The diffraction pattern of **II** (Figure 2S) first appeared to be close to that of Cu_2ZnSnS_4 (PDF 010-75-4122 [48]). However, it should be taken into account that the X-ray diffraction patterns of Cu_2ZnSnS_4 and Cu_2SnS_3 are very similar and can differ quite correctly only at higher diffraction angles 2θ. With the precision scanning in the wide range of 2θ = 90-120°, it is found that sample **II** contains the CZTS and Cu_2SnS_3 (PDF 010-89-4714 [49] phases. The microscopic examination of the polished section revealed some inclusions of the ZnS phase. This suggests that there is no chemical reaction between CZTS and the $ZnCl_2$ flux with the Cl^- ion incorporation. On the other hand, the coexistence of three phases CZTS, Cu_2SnS_3 and ZnS suggests that the beginning of crystallization with the taken CZTS/solvent ratio is still above the CZTS peritectic decomposition temperature. Thus, it can be reasonably assumed that the Cu_2ZnSnS_4-$ZnCl_2$ system is appropriate for the CZTS growth and the phase pure crystals could be obtained at optimal conditions.

The XRD pattern of sample **III** is shown in Figure 2. All diffraction peaks at the 2θ = 10-70° range can be successfully attributed to the known structure of Cu_2ZnSnS_4 [48]. Small unindexed peaks were revealed only at high diffraction angles 2θ = 90-120°. Thus, it can be supposed that sample **III** contains phases with similar parameters or their structure is slightly different from the known one. The absence of foreign phase inclusions is confirmed by the microscopic examination of crystal **III** polished sections in scanning electron and optical microscopes. The images are shown in Figures 1b and 1c, respectively. In both cases, the contrast is uniform, and it verifies the uniform element distribution over the crystal bulk. According to EDX measurements, the internal distribution of chemical components in the grains of **III** is homogeneous with the constituent element ratios Cu/(Zn + Sn) ~ 0.96 and Zn/Sn ~ 1.11 (Table 1). It should be mentioned that the obtained cation ratio lies in the field of CZTS compositions showing the highest solar energy conversion efficiency [23]. Also one should note that the use of $SnCl_2$ as a solvent does not affect the tin content in the final product (see Table 1). It can be assumed that the change in the concentrations of other cations is caused by the peculiarities of their dissolution coefficients in

View Article Online
DOI: 10.1039/D0CE01264E

$SnCl_2$. Generally, the best result in the crystal quality is obtained for the solvent with a relatively low melting temperature ($SnCl_2$, 247°C), and this parameter may be among the key factors for the optimal solvent selection.

The selected crystal **III** was used for the crystal structure determination by the X-ray structure analysis under the constrained chemical composition $Cu_{1.94}Zn_{1.06}SnS_4$, as obtained by EDX measurements. The main crystallographic parameters and refinement details are presented in Table 2. Formally, $Cu_{1.94}Zn_{0.06}SnS_4$ crystallizes in disordered kesterite-type structure [50]. This tetragonal structure could be composed from the cubic sphalerite–ZnS type structure by doubling the sphalerite unit cell along axis c, with unit-cell parameters close to a = 5.44 and c = 10.85 Å [51]. Cationic layers are alternating along the c-axis: Cu/Sn located at z = 0 and z =1/2 (2a and 2b Wyckoff positions, respectively) and Cu/Zn at z = 1/4 and z =3/4 (4d sites), separated by sulfur layers (see Figure 3). The possibility of disordered kesterite-type structure formation for $Cu_{2-x}Zn_{1+x}SnS_4$ was established [52]. Because Cu^{2+} and Zn^{2+} cations have very close atomic scattering factors, it is definitely impossible to distinguish the ordered and disordered kesterite structures from X-ray diffraction experiments, even on single crystals. The extra-content of Zn in this Zn-rich crystal was proved by the EDX determination and it provides the structure refinement with a low R-factor (Table 2). The supplementary data CCDC 2025030 contain the crystallographic data determined for the $Cu_{1.94}Zn_{1.06}SnS_4$ sulfide. These data can be obtained free of charge via http://www.ccdc.cam.ac.uk/conts/retrieving.html, or from the Cambridge Crystallographic Data Centre, 12 Union Road, Cambridge CB2 1EZ, UK; fax: (+44)1223-336-033; or e-mail: deposit@ccdc.cam.ac.uk.

The structural data revealed by the single crystal X-ray diffraction analysis were used for the Rietveld refinement of the XRD pattern recorded for sample **III**. The difference pattern is shown in Figure 2. All diffraction peaks were successfully attributed to the $Cu_{1.94}Zn_{1.06}SnS_4$ phase. The cell parameters refined by Rietveld method are *a* = 5.4324(3) and *c* = 10.8383(2) Å (R_{exp} = 1.74%, R_p =

View Article Online
DOI: 10.1039/D0CE01264E

3.67%, R_{wp} = 6.03%). Some difference between experimental and calculated patterns may be caused by preferential orientation of microcrystals.

The phase purity and homogeneity of sample **III** were additionally tested by Raman measurements. For this purpose, the biggest plate-like crystal was selected. The SEM image of this crystal is shown in Figure 3S. The homogeneous contrast observed for the plate indicates the uniform chemical composition even for the mm-sized crystal. The Raman spectrum of the CZTS single crystal obtained in the frequency range from 100 cm^{-1} to 450 cm^{-1} without selection in polarization is shown in Figure 4. This spectrum looks qualitatively similar to the kesterite spectra measured in [27,51,54]. In the spectrum, one can see strong Raman lines at 167, 289, 338, 375 cm^{-1} and relatively weak peaks at 256 and 348 cm^{-1}. According to [53], the lines at 289 and 338 cm^{-1} can be interpreted as A symmetry modes and peaks at 167, 256 and 348 cm^{-1} can be attributed to E and B symmetry modes. The line at 375 cm^{-1} can be assigned as the LO component of B symmetry modes [23,50]. By applying the polarized excitation beam, a Raman line intensity redistribution was observed for different spatial points of the CZTS plate. This suggests a domain structure on the scale of 50 μm (beam diameter). In general, the Raman spectrum shown in Figure 4 looks very similar to those presented in [27,53,54], taking into account the possible variation of crystallographic orientation. The observed Raman line positions, together with those reported in the literature, are listed in Table 4 [23,49-51]. It is known that the statistical disorder in the cation sublattice is accompanied by a Raman line shift from 337 to 331 cm^{-1} [56]. Thus, the lack of 331 cm^{-1} line contribution to the Raman spectrum of our sample (Figure 4) proves the true kesterite structure of the CZTS sample **III**. Another parameter of this line related to disorder is its line width. It is believed that the line width is related to phonon localization due to lattice disorder [57]. The line full width at half maximum (FWHM) being 11-14 cm^{-1} was reported for CZTS thin films and 10-11 cm^{-1} - for single crystals [57]. In sample **III**, the 337 cm^{-1} line FWHM was as low as 9.6 cm^{-1}, and that corresponds to the lowest known room-temperature value for CZTS crystals, to the best of our knowledge. Thus, the minimal lattice disorder can be reasonably assumed in CZTS

crystal **III**.

View Article Online
DOI: 10.1039/D0CE01264E

4. Conclusions

In the present work, the homogeneous CZTS crystals were obtained from the $SnCl_2$-based flux. The chlorine incorporation in the crystal bulk was not observed, while tin is a constituent of the CZTS crystal. The small grown crystals are characterized by high structural quality. However, the big crystals may be twinned and the optimization of growth conditions seems to be topical to reach big-sized single crystals. This approach may favor the progress of CZTS production for sputtering targets and "monograin" solar cells. On the other hand, the microscale domain structure should be well studied in order to reveal its effect on the electrophysical performance.

Acknowledgements

This work was supported by the Russian Science Foundation (project 19-42-02003), Ministry of Science and Higher Education of Russia (project 075-15-2020-797 (13.1902.21.0024)), the Science Committee of the Ministry of Education and Science of the Republic of Kazakhstan (Grant No. AP08052719), state contract of IGM SB RAS, Russian Ministry of Science and High Education (AAAA-A17-117052410033-9) and DST-RSF Bilateral Project (No. DST/INT/RUS/RSF/P-20 dated May 16, 2019).

References

View Article Online
DOI: 10.1039/D0CE01264E

1. Kee-Jeong Yang, Jun-Hyoung Sim, Dae-Ho Son, Dae-Hwan Kim, Gee Yeong Kim, William Jo, Soomin Song, JunHo Kim, Dahyun Nam, Hyeonsik Cheong and Jin-Kyu Kang, Effects of the compositional ratio distribution with sulfurization temperatures in the absorber layer on the defect and surface electrical characteristics of Cu_2ZnSnS_4 solar cells, Prog. Photovolt: Res. Appl. 23 (2015) 1771–1784.
2. Mario Lang, Tobias Renz, Niklas Mathes, Markus Neuwirth, Thomas Schnabel, Heinz Kalt, Michael Hetterich, Influence of the Cu Content in $Cu_2ZnSn(S,Se)_4$ solar cell absorbers on order-disorder related band gap changes, Appl. Phys. Lett. 109 (2016) 142103.
3. Andrea Crovetto, Andrea Cazzaniga, Rebecca Bolt Ettlinger, Jørgen Schou, Ole Hansen, Large process-dependent variations in band alignment and interface band gaps of Cu_2ZnSnS_4/CdS solar cells, Solar Energy Mater. Solar Cells 187 (2018) 233-240.
4. Louis Grenet, Md Abdul Aziz Suzon, Fabrice Emieux, Frédéric Roux, Analysis of failure modes in kesterite solar cells, ACS Appl. Energy Mater. 1 (5) (2018) 2103-2113.
5. Brajendra S. Sengar, Vivek Garg, Amitesh Kumar, Vishnu Awasthi, Shailendra Kumar, Victor V. Atuchin, Shaibal Mukherjee, Band alingment of Cd-free (Zn, Mg)O layer with $Cu_2ZnSn(S,Se)_4$ and its effect on the photovoltaic properties, Opt. Mater. 84 (2018) 748-756.
6. Tuan V. Vu, A.A. Lavrentyev, B.V. Gabrelian, Hien D. Tong, V.A. Tkach, O.V. Parasyuk, O.Y. Khyzhun, A theoretical and experimental study of the valence-band electronic structure and optical constants of quaternary copper mercury tin sulfide, Cu_2HgSnS_4, a potential material for optoelectronics and solar cells, Opt. Mater. 96 (2019) 109296.
7. Tuan V. Vu , A.A. Lavrentyev, B.V. Gabrelian, V.A. Tkach, Khang D. Pham, O.V. Marchuk, O.V. Parasyuk, O.Y. Khyzhun, First-principles DFT computation and X-ray spectroscopy study of the electronic band structure and optical constants of Cu_2HgGeS_4, Solid State Sci. 104 (2020) 106287.

View Article Online
DOI: 10.1039/D0CE01264E

8. B.V. Gabrelian, A.A. Lavrentyev, Tuan V. Vu, V.A. Tkache, O.V. Marchuk, K.F. Kalmykov, L.N. Ananchenko, O.V. Parasyuk, O.Y. Khyzhun, Quaternary $Cu_2HgGeSe_4$ selenide: Its electronic and optical properties as elucidated from TB-mBJ band-structure calculations and XPS and XES measurements, Chem. Phys. 536 (2020) 110821.
9. Tuan V. Vu, A.A. Lavrentyev, B.V. Gabrelian, Hien D. Tong, V.A. Tkach, O.V. Parasyuk, O.Y. Khyzhun, Simulation within a DFT framework and experimental study of the valence-band electronic structure and optical properties of quaternary selenide $Cu_2HgSnSe_4$, Optik 202 (2020) 163709.
10. Byungha Shin, Oki Gunawan, Yu Zhu, Nestor A. Bojarczuk, S. Jay Chey and Supratik Guha, Thin film solar cell with 8.4% power conversion efficiency using an earth-abundant Cu_2ZnSnS_4 absorber, Prog. Photovolt: Res. Appl. 21 (2013) 72–76.
11. Wei Wang, Mark T. Winkler, Oki Gunawan, Tayfun Gokmen, Teodor K. Todorov, Yu Zhu, david B. Mitzi, Device characteristics of CZTSSe thin-film solar cells with 12.6% efficiency, Adv. Energy Mater. 4 (7) (2014) 1301465.
12. Myeng Gil Gang, Seung Wook Shin, Chang Woo Hong, K. V. Gurav, Jihye Gwak, Jae Ho Yun, Jeong Yong Lee, Jin Hyeok Kim, Sputtering processed highly efficient $Cu_2ZnSn(S,Se)_4$ solar cells by a low-cost, simple, environmentally friendly, and up-scalable strategy, Green Chem. 18 (2016) 700-711.
13. Kee-Jeong Yang, Dae-Ho Son, Shi-Joon Sung, Jun-Hyoung Sim, Young-Ill Kim, Si-Nae Park, Dong-Hwan Jeon, JungSik Kim, Dae-Kue Hwang, Chan-Wook Jeon, Dahyun Nam, Hyeonsik Cheong, Jin-Kyu Kang, Dae-Hwan Kim, A band-gap-graded CZTSSe solar cell with 12.3% efficiency, J. Mater. Chem. A 4 (2016) 10151-10158.
14. Martin A. Green, Yoshihiro Hishikawa, Wilhelm Warta, Ewan D. Dunlop, Dean H. Levi, Jochen Holm-Ebinger, Anita W.Y. Ho-Baillie, Solar cell efficiency tables (version 50), Prog. Photovolt: Res. Appl. 25 (2017) 668–676.

15. C.V. Ramana, S. Utsunomiya, R.S. Ewing, U. Becker, V.V. Atuchin, V.Sh. Aliev, V.N. Kruchinin, Spectroscopic ellipsometry characterization of the optical properties and thermal stability of ZrO_2 films made by ion-beam assisted deposition, Appl. Phys. Lett. 92 (2008) 011917.

16. C.V. Ramana, R.S. Vemuri, V.V. Kaichev, V.A. Kochubey, A.A. Saraev, V.V. Atuchin, X-ray photoelectron spectroscopy depth profiling of La_2O_3/Si thin films deposited by reactive magnetron sputtering, ACS Appl. Mater. Interfaces 3 (2011) 4370-4373.

17. V.V. Atuchin, M.S. Lebedev, I.V. Korolkov, V.N. Kruchinin, E.A. Maksimovskii, S.V. Trubin, Composition-sensitive growth kinetics and dispersive optical properties of thin $Hf_xTi_{1-x}O_2$ ($0 \leq x \leq 1$) films prepared by the ALD method, J. Mater. Sci.: Mater. Elect. (2018) DOI: 10.1007/s10854-018-0351-z.

18. Thomas Schnabel, Erik Ahlswede, On the interface between kesterite absorber and Mo back contact and its impact on solution-processed thin-film solar cells, Sol. Energy Mat. Solar Cells 159 (2017) 290-295.

19. Om Pal Singh, Kuldeep Singh Gour, Rahul Parmar, Vidya Nand Singh, Sodium induced grain growth, defect passivation and enhancement in the photovoltaic properties of Cu_2ZnSnS_4 thin film solar cell, Mater. Chem. Phys. 177 (2016) 293-298.

16. Vishnu Awasthi, Sushil K. Pandey, Saurabh K. Pandey, Shruti Verma, Mukul Gupta, Shaibal Mukherjee, Growth and characterizations of dual ion beam sputtered CIGS thin films for photovoltaic applications, J. Mater. Sci.: Mater. Elect. 25 (7) (2014) 3069-3076.

17. Xin Xu, Shurong Wang, Xun Ma, Shuai Yang, Yaobin Li, Zhen Tang, Optimization of sulfurization time for properties of Cu_2ZnSnS_4 films and cells by sputtering method, J. Mater. Sci.: Mater. Elect. 29 (22) (2018) 19137-19146.

18. Marjana Dimitrievska, Aandrew Fairbrother, Edgardo Saucedo, Alejandro Pérez-Rodríguez, Victor Izquierdo-Roca, Secondary phase and Cu substitutional defect dynamics in kesterite solar cells: Impact on optoelectronic properties, Solar Energy Mater. Solar Cells, 149 (2016) 304-309.

19. Shiyou Chen, Aron Walsh, Xin-Gao Gong, Su-Huai Wei, Classification of lattice defects in the kesterite Cu_2ZnSnS_4 and $Cu_2ZnSnSe_4$ earth-abundant solar cell absorbers, Adv. Mater. 25 (11) (2013) 1522-1539.

20. Brajendra S. Sengar, Vivek Garg, Amitesh Kumar, Shailendra Kumar, Shaibal Mukherjee, Surface layer investigation of dual ion beam sputtered $Cu_2ZnSn(S,Se)_4$ thin film for open circuit voltage improvement, J. Phys. D: Appl. Phys. 51 (2018) 31LT01.

21. Akira Nagaoka, Kenji Yoshino, Hiroki Taniguchi, Tomoyasu Taniyama, Koichi Kakimoto, Hideto Miyake, Growth and characterization of Cu_2ZnSnS_4 single crystals, Phys. Stat. Sol. A 210 (7) (2013) 1328-1331.

22. Slawomir Podsiadlo, Maciej Bialoglowski, Grzegorz Matyszczak, Paulina Marek, Wojciech Gebicki, Rajmund Bacewicz, Marcin Stachowicz, Piotr Dluzewski, Krzysztof Wozniak, Synthesis of bulk kesterite – a prospective photovoltaic material, Eur. J. Inorg. Chem. 2014 (2014) 4730–4733.

23. Maxim Guc, Sergiu Levcenko, Ivan V. Bodnar, Victor Izquierdo-Roca, Xavier Fontane, Larisa V. Volkova, Ernest Arushanov, Alejandro Perez-Rodriguez, Polarized Raman scattering study of kesterite type Cu_2ZnSnS_4 single crystals, Sci. Reports 6 (2015) 19414.

24. I.V. Bodnar, Temperature dependence of the band gap of Cu_2ZnSnS_4 single crystals, Semiconductors 49 (5) (2015) 582-585.

25. Akira Nagaoka, Ryoji Katsube, Shigeru Nakatsuka, Kenji Yoshino, Tomoyasu Taniyama, Hideto Miyake, Koichi Kakimoto, Michael A. Scarpulla, Yoshitaro Nose, Growth and characterization of $Cu_2ZnSn(SxSe_{1-x})_4$ single crystal grown by traveling heater method, J. Cryst. Growth 423 (2015) 9-15.

26. Tat Ming Nga, Mark T. Weller, Gabriela P. Kissling, Laurence M. Peter, Phillip Dale, Finn Babbe, Jessica de Wild, Bernard Wenger, Henry J. Snaith, David Lan, Optoelectronic and spectroscopic characterization of vapour-transport grown Cu_2ZnSnS_4 single crystals, J. Mater. Chem. A 5 (3) (2017) 1192-1200.

27. Akira Nagaoka, Taizo Masuda, Shintaro Yasui, Tomoyasu Taniyama, Yoshitaro Nose, The single-crystal multinary compound Cu_2ZnSnS_4 as an environmentally friendly high-performance thermoelectric material, Appl. Phys. Express 11 (2018) 051203.

28. K. Timmo, M. Kauk-Kuusik, M. Pilvet, T. Raadik, M. Altosaar, M. Danilson, M. Grossberg, J. Raudoja, K. Emits, Influence of order-disorder in Cu_2ZnSnS_4 powders on the performance of monograin layer solar cells, Thin Solid Films 633 (2017) 122-126.

29. K. Timmo, M. Altosaar, J. Raudoja, M. Grossberg, M. Danilson, O. Volobujeva, E. Mellikov, Chemical etching of $Cu_2ZnSn(S,Se)_4$ monograin powder, Proc. IEEE Phot. Spec. Conf. (2010) 1982-1985.

30. A. Weber, R. Mainz, H.W. Schock, On the Sn loss from thin films of the material system Cu-Zn-Sn-S in high vacuum, J. Appl. Phys. 107 (2010) 013516.

31. Alex Redinger, Dominik M. Berg, Phillip J. Dale, Rabie Djemour, Levent Gütay, Tobias Eisenbarth, Nathalie Valle, Susanne Siebentritt, Route toward high-efficiency single-phase $Cu_2ZnSn(S,Se)_4$ thin-film solar cells: Model experiments and literature review, IEEE J. Photovoltaics 1 (2) (2011) 200-206.

32. Alex Redinger, Dominik M. Berg, Phillip J. Dale, Susanne Siebentritt, The consequences of kesterite equilibria for efficient solar cells, J. Am. Chem. Soc. 133 (2011) 3320-3323.

33. G. Nkwusi, I. Leinemann, J. Raudoja, V. Mikli, E. Karba, M. Altosaar, Impact of growth-synthesis conditions on $Cu_2Zn_{1-x}Cd_xSnS_4$ monograin material properties, Superlattice Microst. 98 (2016) 400-405.

34. Powder Diffraction File, release 2010, International Centre for Diffraction Data, Pennsylvania, USA.

35. A.A. Coelho, TOPAS and TOPAS-Academic: an optimization program integrating computer algebra and crystallographic objects written in C++, J. Appl. Cryst. 51 (2018) 210-218.

36. Bruker AXS Inc. (2000-2012). APEX2 (Version 2012.2-0), SAINT (Version 8.18c), and SADABS (Version 2008/1). Bruker Advanced X-ray Solutions, Madison, Wisconsin, USA.

37. George M. Sheldrick, Crystal structure refinement with *SHELXL*, Acta Crystallogr. C 71 (2015) 3-8.

View Article Online
DOI: 10.1039/D0CE01264E

38. I.D. Olekseyuk, I.V. Dudchak, L.V. Piskach, Phase equilibria in the Cu_2S-ZnS-SnS_2 system, J. Alloys Compd. 368 (2004) 135-143.
39. Handbook of Chemistry and Physics, 71st edition, CRC Press, Ann Arbor, Michigan, 1990.
40. Helmer Fjellvåg, Fradrik Gronvold, Svein Stølen, Low-temperature structural distortion in CuS, Z. Kristallogr. 184 (1988) 111-121.
41. M.Kh. Rabadanov, A.A. Loshmanov, Yu.V. Shaldin, Anharmonic thermal vibrations of atoms in crystals with sphalerite structure – GaP, ZnS, SnSe, and ZnTe: High-temperature X-ray structure studies, Cryst, Reports 42 (4) (1997) 592-602.
42. S. Hull, D.A. Keen, High-pressure polymorphism of the copper(I) halides: A neutron-diffraction study to ~10 GPa, Phys. Rev. B 50 (1994) 5868-5885.
43. Georg Will, Ekkehard Hinze, Abdel Rahman M. Abdelrahman, Crystal structure analysis and refinement of digenite, $Cu_{1.8}S$, in the temperature range 20 to 500 °C under controlled sulfur partial pressure, Eur. J. Mineral. 14 (2002) 591-598.
44. Paola Bonazzi, Luca Bindi, Gian Piero Bernardini, Silvio Menchetti, A model for the mechanism of incorporation of Cu, Fe and Zn in the stannite-këesterite series, Cu_2FeSnS_4 – Cu_2ZnSnS_4. Can. Miner. 41 (2003) 639-647.
45. Xue-an Chen, Hiroaki Wada, Akira Sato, Masahiro Mieno, Synthesis, electrical conductivity, and crystal structure of $Cu_4Sn_7S_{16}$ and structure refinement of Cu_2SnS_3, J. Solid State Chem. 139 (1998) 144-151.
46. Alain Lafond, Léo Choubrac, Catherine Guillot-Deudon, Pierre Fertey, Michel Evain, Stéphane Jobic, X-ray resonant single-crystal diffraction technique, a powerful tool to investigate the kesterite structure of the photovoltaic Cu_2ZnSnS_4 compound, Acta Cryst. B 70 (2014) 390-394.
47. V.V. Atuchin, S.V. Borisov, S.A. Magaril, N.V. Pervukhina, Sphalerite framework in polar sulfides, J. Chem. Crystallog. 43 (9) (2013) 488-492.

View Article Online
DOI: 10.1039/D0CE01264E

48. A. Ritscher, M. Hoelzel, M. Lerch, The order-disorder transition in Cu_2ZnSnS_4 - A neutron scattering investigation, J. Solid State Chem. 238 (2016) 68-73.

49. X. Fontané, V. Izquierdo-Roca, E. Saucedo, S. Schorr, V.O. Yukhymchuk, M.Ya. Valakh, A. Perez-Rodriguez, J.R. Morante, Vibrational properties of stannite and kesterite type compounds: Raman scattering analysis of $Cu_2(Fe,Zn)SnS_4$, J. Alloy Compd. 539 (2012) 190-194.

50. Marjana Dimitrievska, Federica Boero, Alexander P. Litvinchuk, Simona Delsante, Gabriella Borzone, Alejandro Pérez-Rodríguez, Victor Izquierdo-Roca, Structural polymorphism in "kesterite" Cu_2ZnSnS_4: Raman spectroscopy and first-principles calculations analysis, Inorg. Chem. 56 (6) (2017) 3467-3474.

51. Dumitru Dumcenco, Ying-Sheng Huang, The vibrational properties study of kesterite Cu_2ZnSnS_4 single crystals by using polarization dependent Raman spectroscopy, Opt. Mater. 35 (3) (2013) 419-425.

52. M.Y. Valakh, O.F. Kolomys, S.S. Ponomaryov, V.O. Yukhymchuk, I.S. Babichuk, V. Izquiero-Roca, E. Saucedo, A. Perez-Rodriguez, J.R. Morante, S. Schorr, I.V. Bodnar, Raman scattering and disorder effect in Cu_2ZnSnS_4, Phys. Stat. Sol. RRL 7 (4) (2013) 258-261.

53. S. Levcenko, V.E. Tezlevan, E. Arushanov, S. Schorr, T. Unold, Free-to-bond recombination in near stoichiometric Cu_2ZnSnS_4 single crystals, Phys. Rev. B 86 (4) (2012) 045206.

Table 1. Chemical compositions of CZTS phase obtained by direct fusion and from $SnCl_2$ flux.

	Cu, at. %	Zn, at. %	Sn, at. %	S, at. %	Cu/(Zn+Sn)	Zn/Sn
Direct synthesis	25,49	12,59	12,05	49,87	1,03	1,05
$SnCl_2$ flux	24,43	13,38	12,06	50,13	0,96	1,11

Table 2. Crystal data and structure refinement for $Cu_{1.94}S_4SnZn_{1.06}$

View Article Online
DOI: 10.1039/D0CE01264E

Empirical formula	$Cu_{1.94}S_4SnZn_{1.06}$
Formula weight	439.49
Crystal system	Tetragonal
Space group	I-42m
Unit cell dimensions	$a = b = 5.4383(2)$ Å
	c = 10.8455(5) Å
Volume	320.76(3) Å^3
Z	2
Density (calculated)	4.550 M/cm^3
Absorption coefficient	15.276 mm^{-1}
Crystal size	0.12 x 0.10 x 0.02 mm^3
Theta range for data collection	3.757 – 32.630°
Index ranges	-8 ≤ h ≤ 6 -5 ≤ k ≤ 8 -15 ≤ l ≤ 16
I_{hkl} coll.	1592
$I_{hkl} > 2\sigma_I (R_{int})$	335 (0.0294)
Completeness to theta = 25.25°	99.1 %
Data / restraints / parameters	335 / 0 / 15
Goodness-of-fit on F^2	1.053
R ($I > 2\sigma_I$)	$R_1 = 0.0092$, $wR_2 = 0.0224$
R (I_{hkl} coll.)	$R_1 = 0.0092$, $wR_2 = 0.0224$
Absolute structure parameter	0.02(4)
Largest diff. peak and hole	0.352 and -0.488 e/Å^3

View Article Online
DOI: 10.1039/D0CE01264E

Table 3. Wavenumber and mode assignment of Raman peaks of the Cu_2ZnSnS_4 sample **III** and related literature data

This work (cm^{-1})	Symmetry	Ref. [49] (cm^{-1})	Ref. [23] (cm^{-1})	Ref. [50] (cm^{-1})	Ref. [51] (cm^{-1})
167	E/B	166	167	165.9	160–162
256	E/B	252	250	252.1	245–255
289	A	287	287	283.2	285
338	A	337	338	336.3	334
348	E/B	347	347		241–353
375	B(LO)		374	375.9	

Captions

View Article Online
DOI: 10.1039/D0CE01264E

Figure 1. (a) CZTS sample obtained by the direct fusion of elementary compounds and after the recrystallization with the $SnCl_2$ flux (b,c). The images are obtained in optical (a, b) and scanning electron (c) microscopes.

Figure 2. X-ray diffraction data for CZTS obtained from $SnCl_2$: a) comparison of experimental (black) and Rietveld refined (red) data, b) difference curve.

Figure 3. Fragment of the structure of $Cu_{1.94}Zn_{0.06}SnS_4$. The unit cell is outlined. The lone metal atoms are omitted for clarity.

Figure 4. Raman spectrum of the Cu_2ZnSnS_4 sample. The Raman lines are marked with arrows.

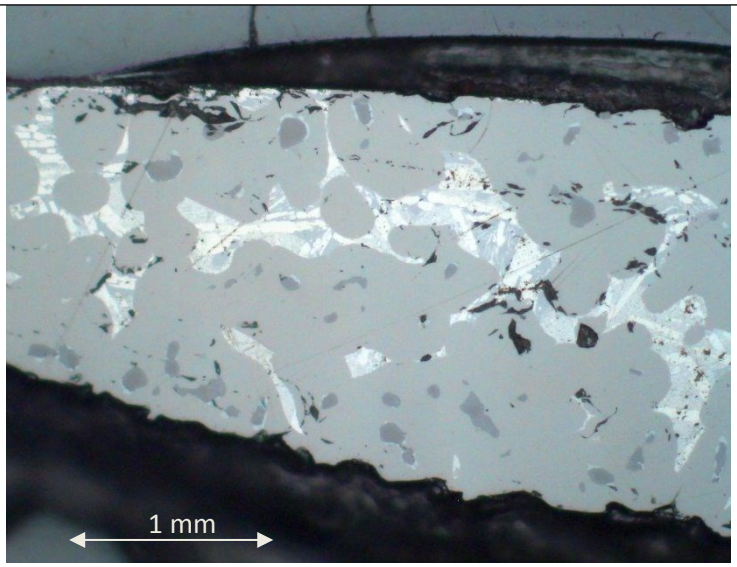

a

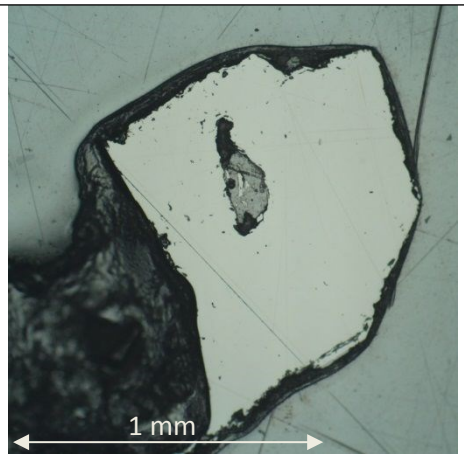

b

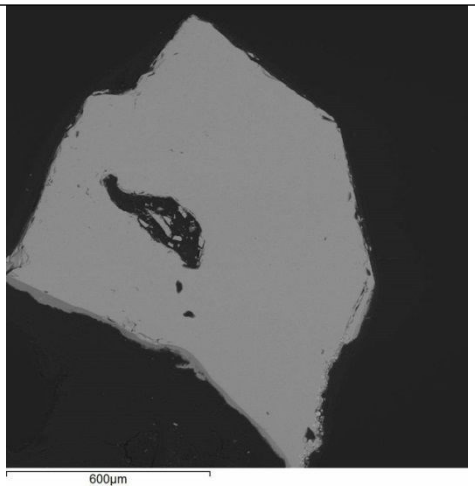

c

Figure 1

View Article Online
DOI: 10.1039/D0CE01264E

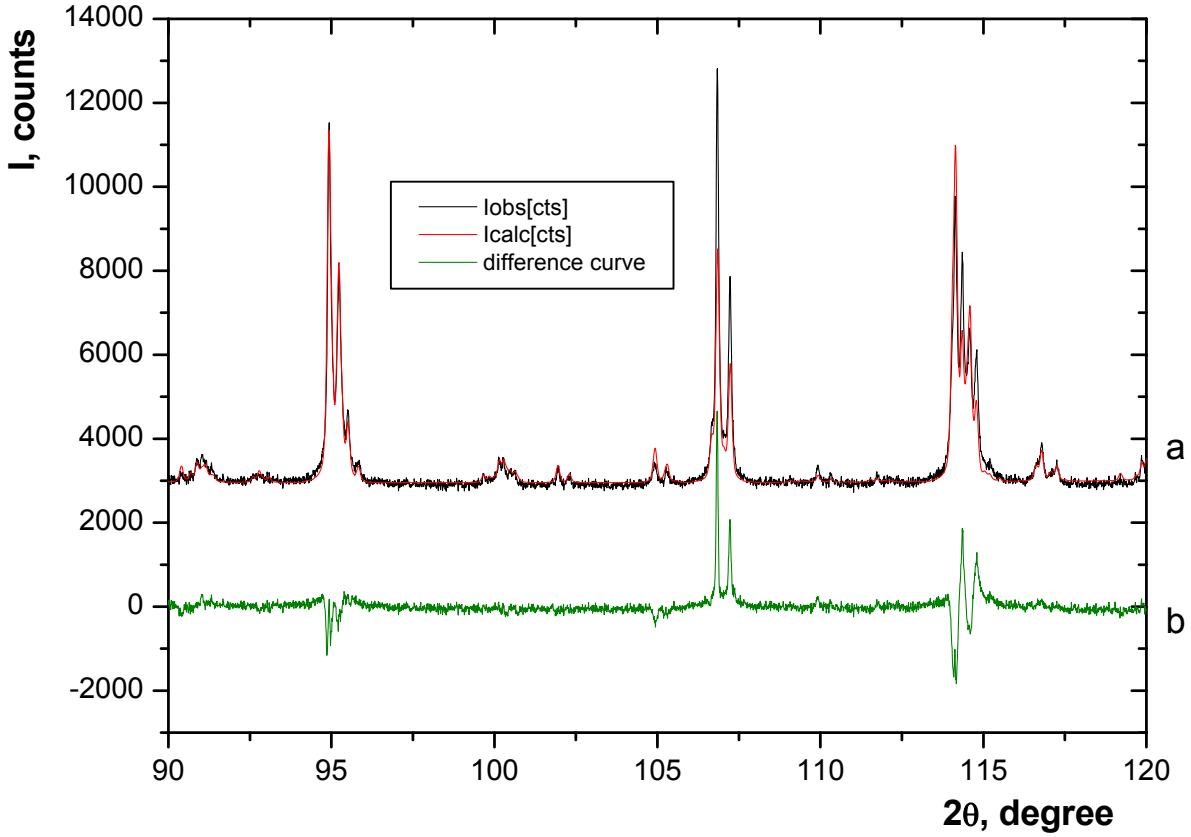

Figure 2

View Article Online
DOI: 10.1039/D0CE01264E

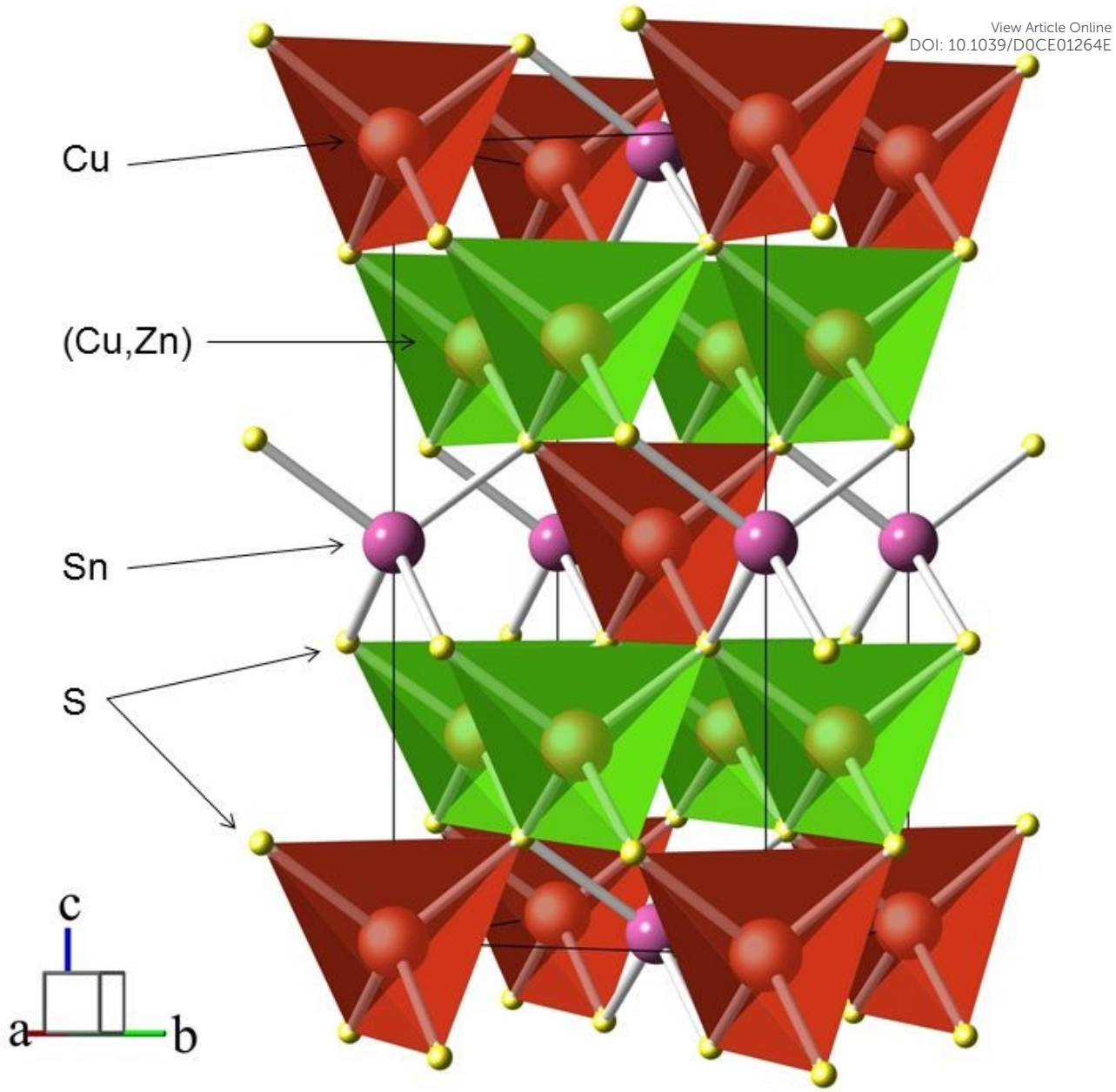

Figure 3

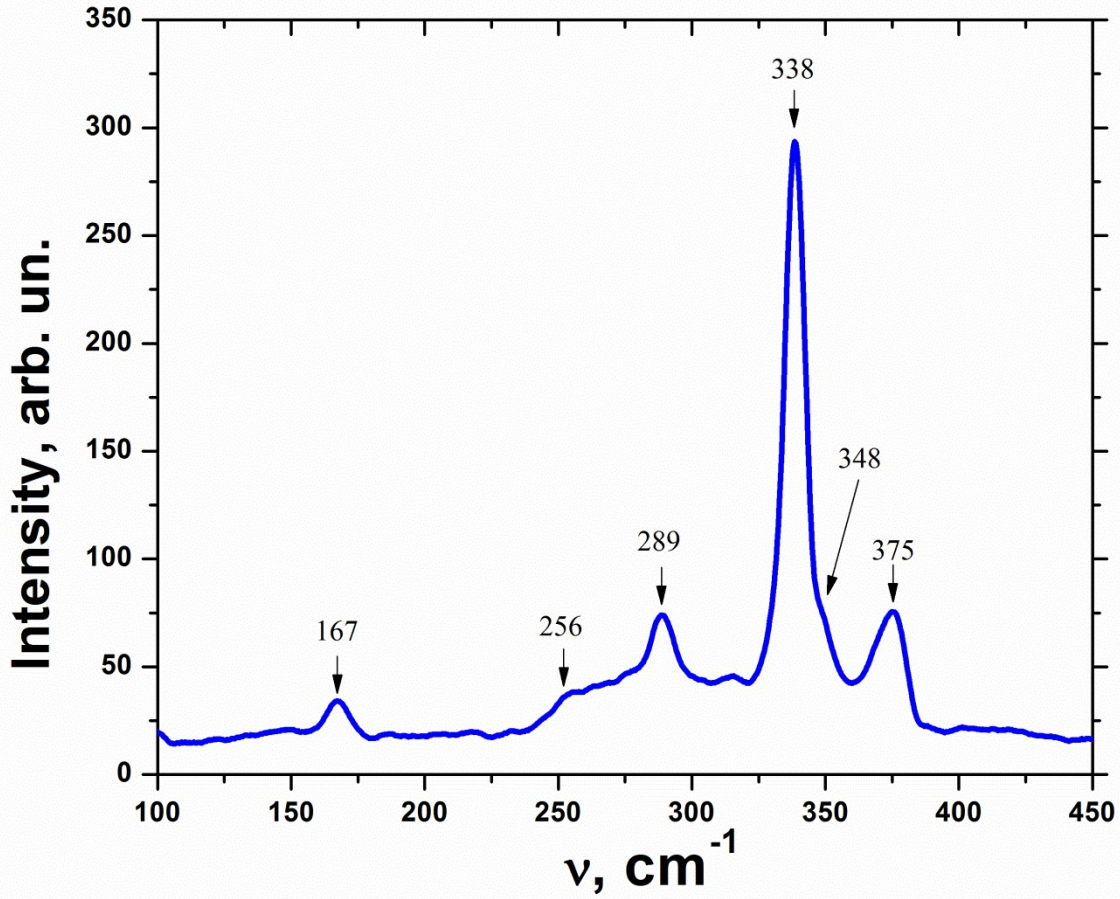

Figure 4

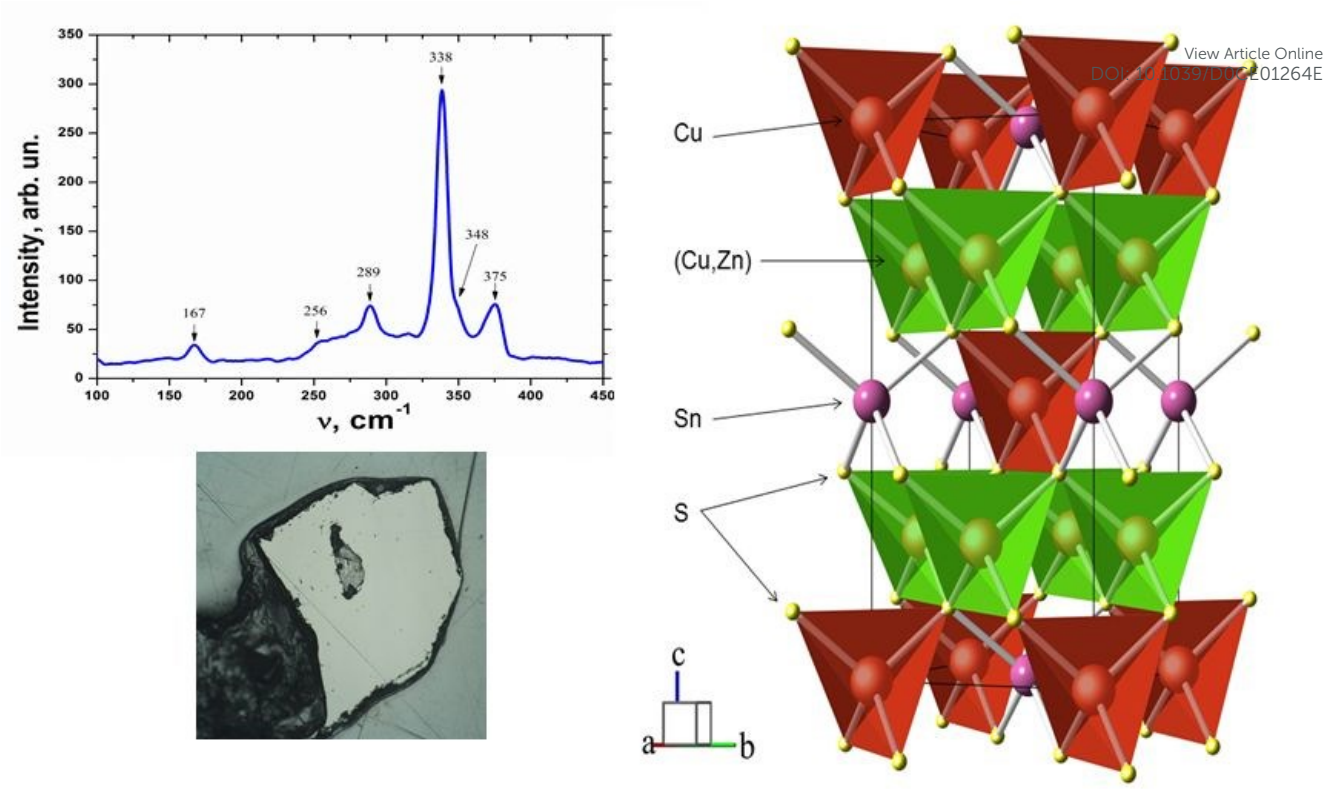

Single crystal growth of Cu_2ZnSnS_4 in $SnCl_2$-based flux.